International Journal for Parasitology: Drugs and Drug Resistance 7 (2017) 12–22

Contents lists available at ScienceDirect

International Journal for Parasitology: Drugs and Drug Resistance

journal homepage: www.elsevier.com/locate/ijpddr

(S)-5-ethynyl-anabasine, a novel compound, is a more potent agonist than other nicotine alkaloids on the nematode *Asu*-ACR-16 receptor

Fudan Zheng [a], Xiangwei Du [a], Tsung-Han Chou [b], Alan P. Robertson [c], Edward W. Yu [b], Brett VanVeller [a], Richard J. Martin [c, *]

[a] Department of Chemistry, College of Liberal Arts and Sciences, Iowa State University, Ames, IA, USA
[b] Department of Physics and Astronomy, College of Liberal Arts and Sciences, Iowa State University, Ames, IA, USA
[c] Department of Biomedical Sciences, College of Veterinary Medicine, Iowa State University, Ames, IA, USA

ARTICLE INFO

Article history:
Received 2 September 2016
Received in revised form
23 November 2016
Accepted 2 December 2016
Available online 9 December 2016

Keywords:
Asu-ACR-16
Agonist-binding site
Nicotine alkaloids
Xenopus expression
Ascaris suum
Anthelmintic

ABSTRACT

Nematode parasites infect ~2 billion people world-wide. Infections are treated and prevented by anthelmintic drugs, some of which act on nicotinic acetylcholine receptors (nAChRs). There is an unmet need for novel therapeutic agents because of concerns about the development of resistance. We have selected *Asu*-ACR-16 from a significant nematode parasite genus, *Ascaris suum*, as a pharmaceutical target and nicotine as our basic moiety (EC_{50} 6.21 ± 0.56 μM, I_{max} 82.39 ± 2.52%) to facilitate the development of more effective anthelmintics.

We expressed *Asu*-ACR-16 in *Xenopus* oocytes and used two-electrode voltage clamp electrophysiology to determine agonist concentration-current-response relationships and determine the potencies (EC_{50}s) of the agonists.

Here, we describe the synthesis of a novel agonist, (S)-5-ethynyl-anabasine, and show that it is more potent (EC_{50} 0.14 ± 0.01 μM) than other nicotine alkaloids on *Asu*-ACR-16. Agonists acting on ACR-16 receptors have the potential to circumvent drug resistance to anthelmintics, like levamisole, that do not act on the ACR-16 receptors.

1. Introduction

Our research has had a focus on nicotinic acetylcholine receptors (nAChRs) of parasitic nematodes because they are target sites that bind a major class of anthelmintic drugs. nAChRs are pentameric ligand-gated ion channels involved in synaptic transmission in the nervous systems of both vertebrates and invertebrates (Taly et al., 2009); these receptor channels also serve other functions including paracrine functions in non-excitable tissues (Proskocil et al., 2004). The nAChRs are activated by the ligand agonists: acetylcholine (ACh), nicotine and structurally related derivatives, that produce opening of their transmembrane ion-channel and flux of sodium, potassium and sometimes calcium ions across the membrane.

The agonist-binding sites of nAChRs have been well studied by photolabeling, mutagenesis and electrophysiology (Arias, 2000). Our understanding of ligand-receptor interactions has improved following co-crystal structure studies of invertebrate acetylcholine binding proteins (AChBPs) with cholinergic ligands (Sixma and Smit, 2003; Rucktooa et al., 2009). AChBPs are homologs of the extracellular agonist-binding site domain of nAChRs that share 20–24% nucleotide sequence identity with the extracellular domain of AChRs (Blum et al., 2010). The agonist-binding site of nAChRs is in the extracellular domain at the interface between the principal subunit (that is an alpha subunit with vicinal cysteines) and the adjacent complementary subunit. Five aromatic amino acids in the agonist-binding site are highly conserved in nAChRs, some of which contribute to the cation-π interactions with the cationic nitrogen in agonists (Dougherty, 2013). Another feature of nAChR agonists is the hydrogen bond acceptor, which is about 4–6 Å from the cationic nitrogen. Based on the high-resolution structures of AChBPs, the hydrogen bond acceptor of the agonist is stabilized by a water molecule, which interacts with the carbonyl or the amide backbones of two less conserved residues (L102 and M114) on loop E of the complementary subunit through three hydrogen bonding interactions (Van Arnam and Dougherty, 2014).

* Corresponding author. Department of Biomedical Sciences, Iowa State University, 1800 Christensen Dr., Ames, IA 50011, USA.
E-mail address: rjmartin@iastate.edu (R.J. Martin).

http://dx.doi.org/10.1016/j.ijpddr.2016.12.001

Ascaris, a genus of clade III nematode parasites, are gastrointestinal roundworms that infect humans, pigs and other animals worldwide (Taylor et al., 2016) and have been estimated to cause more than 1.2 billion human infections (de Silva et al., 2003). In developing countries, the control of *Ascaris* infection relies on the limited number of available anthelmintic drugs. Drug resistance in various nematodes has been reported following frequent use of anthelmintics (Garcia et al., 2016). There is an unmet need for novel effective drugs which would overcome development of resistance to existing anthelmintics.

The ACR-16 nicotinic acetylcholine receptor of *Ascaris suum* (*Asu*-ACR-16) is a nematode homopentameric receptor, which resembles vertebrate α7 nAChRs (Mongan et al., 2002). *Asu*-ACR-16 is widely distributed in *A. suum* tissues but its physiological function remains to be determined (Abongwa et al., 2016; Zheng et al., 2016). As one of the recently characterized nematode parasitic nAChRs, *Asu*-ACR-16 is pharmacologically different to its host α7 nAChR and may be exploited as an anthelmintic drug target to counter resistance to cholinergic anthelmintics directed at other pharmacological types of nAChR (Holden-Dye et al., 2013; Zheng et al., 2016).

The agonist-binding site of *Asu*-ACR-16 receptors can be predicted by homology modeling using the human α7 nAChR chimera as structural template, which shares 38% identity and 73% similarity in amino acid sequence. Five conserved aromatic residues and two hydrogen-bond interacting residues have orientations very close to corresponding residues in other nAChRs, facilitating our investigation of drug-receptor interactions of the *Asu*-ACR-16 receptor (Zheng et al., 2016).

We know that the *Asu*-ACR-16 receptor is sensitive to six nicotinic agonists: nicotine, ACh, cytisine, 3-bromocytisine, epibatidine, dimethyl-4-phenyllpiperazinium iodide (DMPP), but insensitive to other cholinergic anthelmintic agonists (Abongwa et al., 2016). All six of the *Asu*-ACR-16 agonists share the nicotinic pharmacophore: a cationic nitrogen separated by ~5 Å from a hydrogen bond acceptor. Here we use a combination of structural modeling and synthetic strategy based on the nicotinic pharmacophore to explore the pharmacological profiles of nicotine derivatives on the *Asu*-ACR-16 receptor.

2. Materials and methods

2.1. Homology modeling and docking

The *Asu*-ACR-16 sequence is available in UniProtKB under the accession number F1KYJ9 (Wang et al., 2011). Three crystal structures of a human α7 nAChR chimera co-crystalized with ligands of different modes of action were used as templates (Table 1) to build three different bound-form models of the ECD-*Asu*-ACR-16 (Li et al., 2011; Huang et al., 2013; Zheng et al., 2016). Smiles strings of nicotine derivatives were obtained from the ZINC website (http://zinc.docking.org/search/structure) and converted to PDBQT format for our docking studies. Docking of these ligands was performed at the orthosteric ligand-binding sites of agonist-bound, apo (no ligand) and antagonist-bound forms of the ECD-*Asu*-ACR-16 models using AutoDock Vina Software (Trott and Olson, 2010; Zheng et al., 2016). We investigated the intermolecular interactions in our models by comparing the intermolecular distances in the crystal structures and our models ($\leq$ 1 Å difference).

2.2. Expression and electrophysiology of Asu-ACR-16 in oocytes

Full length cRNA of *Asu-acr-16* and the ancillary gene, *Asu-ric-3* (UniProtKB accession number: F1L1D9_ASCSU). were prepared using the previously described methods (Zheng et al., 2016). A cRNA mixture of 25 ng *Asu-acr-16* and 5 ng *Asu-ric-3* cRNA in 50 nL RNAse-free water was injected into de-folliculated *Xenopus laevis* oocytes (Ecocyte Bioscience, Austin, TX, USA). The injected oocytes were incubated in incubation solution (100 mM NaCl, 2 mM KCl, 1.8 mM $CaCl_2 \cdot 2H_2O$, 1 mM $MgCl_2 \cdot 6H_2O$, 5 mM HEPES, 2.5 mM Na pyruvate, 100 U/mL penicillin, 100 μg/mL streptomycin, pH 7.5) at 19 °C for 4–8 days, with 100 μM BAPTA-AM added ~3 h before recording.

A two-electrode voltage-clamp technique was used to record currents from the *Asu*-ACR-16 receptor expressed in the *Xenopus* oocytes. The oocytes were kept in recording solution (100 mM NaCl, 2.5 mM KCl, 1 mM $CaCl_2 \cdot 2H_2O$ and 5 mM HEPES, pH 7.3) and clamped to −60 mV. Inward currents were induced by addition of chemicals that acted as agonists that opened the nicotinic ion-channel receptors. An Axoclamp 2B amplifier (Molecular Devices, CA, and USA) was used to record the currents that were acquired with Clampex 9.2 (Molecular Devices, CA, USA) software and analyzed using GraphPad Prism 5.0 (GraphPad Software Inc. CA, USA).

2.3. Chemicals used for synthesis

The following chemicals were used for the synthesis of (S)-5-bromonicotine, (S)-5-bromoanabsine and (S)-5-ethynyl-anabsine: 4,4'-di-*tert*-butyl-2,2'-dipyridyl (dtbpy), copper (II) bromide ($CuBr_2$), 2-methyl-3-butyn-2-ol, triethylamine (Et_3N) and *N*,*N*-diisopropylethylamine (DIPEA) obtained from Sigma-Aldrich (St Louis, MO, USA); di-μ-methoxobis (1,5-cyclooctadiene)diiridium(I) ($[Ir(COD)(OMe)]_2$) and methanesulfonato (2-di-t-butylphosphino-2′,4′,6'-tri-i-propyl-1,1'-biphenyl) (2'-amino-1,1'-biphenyl-2-yl) palladium (II) ($Pd(PPh_3)_2Cl_2$) obtained from Strem Chemicals (Newburyport, MA, USA); (S)-nicotine, (S)-anabasine and copper(I) iodide (CuI) obtained from Alfa Aesar (Ward Hill, MA, USA); bis(-pinacolato)diboron (B_2pin_2) obtained from Matrix Scientific (Columbia, SC, USA); (trimethylsilyl)acetylene and di-*tert*-butyl dicarbonate (Boc_2O) obtained from Oakwood Products (Estill, SC, USA); dichloromethane (DCM), trifluoroacetic acid (TFA), methanol (MeOH), tetrahydrofuran (THF) and potassium carbonate (K_2CO_3) obtained from Fisher Scientific (Waltham, MA, USA).

2.4. General synthetic experiment

All air-sensitive procedures were conducted under an inert atmosphere of a nitrogen-filled dry box or by standard Schlenk techniques. All reactions were performed under an atmosphere of nitrogen unless otherwise stated. All glassware for moisture

Table 1
Structural information for the ECD-*Asu*-ACR-16 and two of its homologous proteins (human α7 nAChR chimera and *Lst*-AChBP).

protein	Organism	PDB code	Resolution (Å)	Ligand	Pharmacology
ECD-ACR-16	*Ascaris suum*				
α7 nAChR	*Homo sapiens* &	3SQ6	2.8	epibatidine	agonist
chimera	*Lymnaea stagnalis*	3SQ9	3.1	none	none
		4HQP	3.51	α-bungarotoxin	antagonist
AChBP	*Lymnaea stagnalis*	1UW6	2.2	nicotine	agonist

sensitive reactions was dried at 140 °C in an oven. THF and DCM were degassed by purging with argon for 45 min and dried with a solvent purification system by passing through a one-meter column of activated alumina. Flash column chromatography was performed on Fisher brand silica gel 60 (230–400 mesh). Products were visualized on TLC by UV light or by staining with $KMnO_4$, phosphomolybdic acid or ceric ammonium molybdate. HRMS (ESI) analysis was performed at the Iowa State University Chemical Instrumentation Facility on an Agilent 6540 QTOF spectrometer. NMR spectra were acquired on Varian MR-400 and Bruker Avance III 600 spectrometers at the Iowa State University Chemical Instrumentation Facility. Chemical shifts are reported in ppm relative to a residual solvent peak ($CDCl_3$ = 7.26 ppm for ^1H and 77.0 ppm for ^{13}C). Coupling constants are reported in hertz.

2.5. Synthesis of (S)-5-bromonicotine

Synthesis of (S)-5-bromonicotine was carried out following the published procedure (Liskey et al., 2010):

2.6. Synthesis of (S)-tert-butyl-2-(pyridine-3-yl)piperidine-1-carboxylate

Synthesis of compound **-1**, (*S*)-*tert*-butyl 2-(pyridin-3-yl)piperidine-1-carboxylate, below, was conducted using the following approach.

Boc_2O (3.30 g, 15.1 mmol, 1.10 equiv) was added to a solution of (S)-anabasine (2.23 g, 13.7 mmol, 1.0 equiv) and Et_3N (2.10 mL, 15.1 mmol, 1.10 equiv) in THF at 0 °C. The reaction mixture was stirred for 10 min and warmed to room temperature. After stirring for 2 h, the mixture was diluted with water, and extracted with EtOAc (3×). The organic layers were combined, dried over Na_2SO_4 and concentrated under reduced pressure. The crude product was purified by flash column chromatography on silica gel (1:1 hexane:EtOAc) to yield compound −1, (*S*)-*tert*-butyl 2-(pyridin-3-yl) piperidine-1-carboxylate in 95% yield (3.40 g, 13.1 mmol) as a pale yellow liquid (confirmed by ^1H NMR ($CDCl_3$, 400 MHz) δ 1.36–1.69 (m, 4H), 1.46 (s, 9H), 1.91–2.00 (s, 1H), 2.27 (d, J = 14.0 Hz, 1H), 2.69–2.76 (m, 1H), 4.07 (d, J = 14.8 Hz, 1H), 5.47 (br, s, 1H), 7.34–7.38 (m, 1H), 7.63 (d, J = 7.6 Hz, 1H), 8.50 (s, 1H), 8.52 (s, 1H): spectral data matched the literature precedent, (Beng and Gawley, 2011).

2.7. Synthesis of (S)-tert-butyl 2-(5-bromopyridin-3-yl)piperidine-1-carboxylate

Synthesis of compound **-2,** (S)-*tert*-butyl 2-(5-bromopyridin-3-yl)piperidine-1-carboxylate from compound −1 was carried out as described below.

In a nitrogen-filled glove box, compound **-1** (1.31 g, 5.0 mmol), B_2pin_2 (1.12 mg, 4.4 mmol), $[Ir(COD)(OMe)]_2$ (99.5 mg, 0.150 mmol, 0.030 equiv), dtbpy (80.5 mg, 0.030 mmol, 0.060 equiv), and THF (8.0 mL) were combined in a vial. The reaction mixture was then sealed and heated at 80 °C for 16 h. After the reaction mixture was cooled to room temperature, the volatiles were removed under vacuum. The residue was dissolved in 50.0 mL of MeOH and 50.0 mL of distilled water followed by $CuBr_2$ (3.35 g, 15.0 mmol). The flask was then sealed and heated at 80 °C for 16 h. The reaction mixture was cooled to room temperature, and 30% NH_4OH (aq) (20.0 mL) was added to the reaction mixture. The reaction mixture was extracted with EtOAc (3 ×), and the organic layers were combined, washed with brine, and dried over Na_2SO_4. The product was purified by column chromatography using silica gel (3:1 hexane:EtOAc) to give compound **-2**, (*S*)-*tert*-butyl 2-(5-bromopyridin-3-yl)piperidine-1-carboxylate in 36% yield (618 mg, 1.80 mmol) as a pale yellow solid. ^1H NMR (400 MHz, $CDCl_3$) δ 1.30–1.69 (m, 4H), 1.46 (s, 9H), 1.89–1.98 (s, 1H), 2.24 (dd, J = 16.0, 2.0 Hz, 1H), 2.68–2.75 (m, 1H), 4.07 (d, J = 15.6 Hz, 1H), 5.43 (s, 1H), 7.69 (s, 1H), 8.42 (s, 1H), 8.56 (s, 1H); ^{13}C NMR (100.5 MHz, $CDCl_3$) δ 19.2, 25.0, 27.7, 28.3, 40.2, 51.2, 80.2, 120.9, 137.1, 138.1, 146.4, 148.8, 155.2; HRMS (ESI) calcd. For $C_{15}H_{22}BrN_2O_2^+$ $[M+H]^+$ 341.0859, found 341.0864, Fig. S1.

2.8. Synthesis of (S)-5-bromoanabasine

Synthesis of (S)-5-bromoanabasine, was prepared from compound **-2** as described below.

To a solution of compound **2** (93.0 mg, 0.273 mmol, 1.0 equiv) in DCM (5.0 mL), TFA (1.0 mL) was added dropwise. The reaction mixture was stirred at room temperature for 12 h. The mixture was diluted with saturated $NaHCO_3$ and extracted with EA (3×). The organic layers were combined, dried over Na_2SO_4 and concentrated under reduced pressure. The crude product was purified by flash column chromatography on silica gel (10:1 hexane:EtOAc to 10:1 EtOAc:Et_3N) to give (S)-5-bromoanabasine in 83% yield (54.4 g, 0.226 mmol) as a pale yellow solid. ^1H NMR (400 MHz, $CDCl_3$) δ 1.43–1.55 (m, 3H), 1.65–1.68 (m, 1H), 1.75–1.78 (m, 1H), 1.89 (brs, 2 H), 2.74–2.80 (m, 1H), 3.18 (d, J = 11.6 Hz, 1H), 3.61–3.63 (m, 1H), 7.89 (t, J = 1.6 Hz, 1H), 4.7 (d, J = 1.6 Hz, 1H), 8.53 (d, J = 2.0 Hz, 1H); ^{13}C NMR (151.0 MHz, $CDCl_3$) δ 25.0, 25.5, 34.8, 47.4, 59.1, 120.8, 136.9, 142.5, 146.7, 149.6; HRMS (ESI) calcd. For $C_{10}H_{14}BrN_2^+$ $[M+H]^+$ 241.0335, found 241.0332, Fig. S2.

2.9. Synthesis of (S)-5-ethynyl-anabasine

Synthesis of (S)-5-ethynyl-anabasine, was prepared from (S)-5-bromoanabasine as described below.

In a nitrogen-filled Schlenk tube, compound **2** (247 mg, 1.02 mmol) in THF (3.0 mL), $Pd(PPh_3)_2Cl_2$ (143 mg, 0.204 mmol, 0.20 equiv), CuI (39.0 mg, 0.204 mmol, 0.20 equiv), DIPEA (3.0 mL), and trimethylsilylacetylene (0.16 mL, 1.12 mmol, 1.10 equiv) were added. The mixture was stirred at 70 °C for 16 h. After cooled to room temperature, the mixture was filtered through a short pad of silica gel and washed with ethyl acetate The filtrate was concentrated and purified by short silica gel column (100:1 hexane:EtOAc to hexane:EtOAc 5:1) to give the crude product, which was used directly for next step.

To a solution of the crude product in DCM (10.0 mL), TFA (10.0 mL) was added. The mixture was stirred at rt for 2 h. All the volatiles were removed under reduced pressure. The crude product was purified by short silica gel column (2:1 hexane:EtOAc to 8:1 EtOAc:Et_3N).

To a solution of the above crude product in MeOH (10.0 mL), K_2CO_3 (568 mg, 4.08 mmol) was added. The mixture was stirred at room temperature for 16 h. After filtration and concentration, the product was purified by column chromatography using silica gel (5:1 hexane:EtOAc to 10:1 EtOAc:Et_3N) to give **(S)-5-ethynyl-anabasine** in 7% yield (12.8 mg, 0.0714 mmol) as a pale yellow liquid. ^1H NMR (400 MHz, $CDCl_3$) δ 1.45–1.57 (m, 3H), 1.66–1.69 (m, 1H), 1.77–1.79 (m, 1H), 1.90 (brs, 1H), 2.07 (brs, 1H), 2.76–2.81 (m, 1H), 3.18 (s, 1H), 3.19 (d, J = 12.0 Hz, 1H), 3.62–3.65 (m, 1H), 7.84 (t, J = 2.0 Hz, 1H), 8.54 (s, 1H), 8.59 (s, 1H); HRMS (ESI) calculated. For $C_{12}H_{15}N_2^+$ $[M+H]^+$187.1230, found 187.1232, Fig. S3.

2.10. Pharmacological characterization of nicotinic derivatives and data analysis

The aqueous soluble compounds: acetylcholine (ACh), (S)-nicotine, (S)–SIB 1508Y, (S)-1-methylnicotinium, (S)-1'-methylnicotinium, nornicotine, (S)-cotinine, (S)-anabasine, (S, R)-anabasine were dissolved in recording solution at the

concentrations described in the results. Non-polar compounds were dissolved initially in DMSO to make 100 mM stock solutions of each. Subsequently they were diluted in recording solution to give a concentration of DMSO of <0.1%.

100 μM ACh was applied first to each oocyte for 10 s to check for robust *Asu*-ACR-16 expression. In all oocyte recordings the peak current response to 100 μM ACh was used to normalize subsequent current responses in that oocyte. Recording solution was then used to wash out the drug from the oocytes for 3 min prior to next application of drug perfusion.

Nicotine derivatives that elicited inward currents at 100 μM were classed as agonists. To further characterize the nicotine derivative agonists, increasing concentrations of the derivatives were applied for 10 s (3 min wash intervals between drug applications). The resulting dose-response relationships were described by the Hill equation to give estimates of the EC_{50} (μM), Hill slope (n_H), maximum response (I_{max}, %) and expressed as mean ± S.E.M. ($N = 5$) using GraphPad Prism 5.0 (Graphpad Software Inc. CA, USA).

2.11. Drugs

ACh, (−)-nicotine hydrogen tartrate salt ((S)-nicotine), anabasine ((S, R)-anabasine), (±)-nornicotine (nornicotine), 5-(1-methylpyrrolidin-2-yl)-pyridin-2-ylamine dihydrochloride (6-AN) and (−)-cotinine ((S)-cotinine) were purchased from Sigma-Aldrich (St Louis, MO, USA). SIB 1508Y maleate ((S)−SIB 1508Y) was obtained from Tocris Bioscience (Ellisville, MO, USA). (S)-anabasine, rac-5-methylnicotine (5-methylnicotine), S-(−)-nicotine-5-carboxaldehyde ((S)-nicotine-5-carboxaldehyde), (±)-6-methylnicotine (6-methylnicotine), (S)-1-methylnicotinium iodide ((S)-1-methylnicotinium), (S)-1'-methylnicotinium iodide ((S)-1'-methylnicotinium), (R, S)−N-ethyl nornicotine (homonicotine), N-methyl anabasine were purchased from Toronto Research Chemicals (Toronto, ON, Canada).

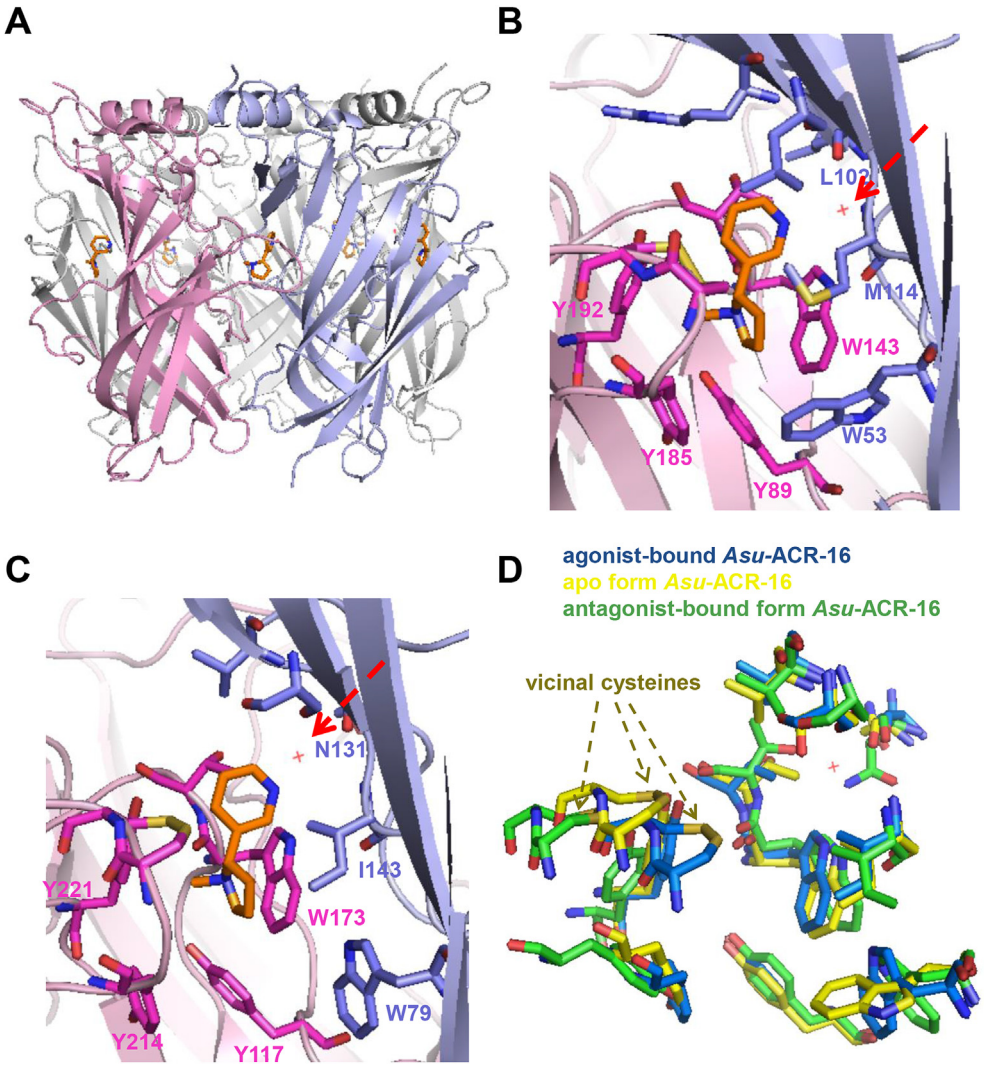

Fig. 1. Crystal structure of *Lst*-AChBP bound with nicotine (PDB code: 1UW6) and the agonist-bound model of *Asu*-ACR-16.
(A) Ribbon diagram of the AChBP co-crystalized with nicotine, as viewed with membrane at the bottom. The principal subunit is highlighted by light pink and the complement subunit is highlighted by light purple, for clarity. Nicotine (orange) is bound in the five ligand-binding sites in the extracellular domain of AChBP.
(B) Close view of the AChBP ligand-binding site. The principal subunit in light pink, the complementary subunit in light purple. Residues interacting with nicotine (orange) are represented as sticks ((+), pink; (−), purple), and water molecule is shown as red dot, view with membrane at the bottom.
(C) Close view of the agonist-bound model of *Asu*-ACR-16 ligand-binding site. The principal subunit in light pink, the complementary subunit in light purple. The interacting residues are represented as sticks ((+), pink; (−), purple), and water molecule is shown as red dot, view with membrane at the bottom. (D) Superposition of residues in agonist-binding site, among agonist-bound form (blue), apo (no ligand) form (yellow), antagonist-bound form (green) of *Asu*-ACR-16 models are shown. (For interpretation of the references to colour in this figure legend, the reader is referred to the web version of this article.)

3. Results

3.1. Ligand-binding sites

Lst-AChBP (PDB code: 1UW6) (Celie et al., 2004) shows 23.33% sequence identity and 64.29% sequence similarity to ECD-*Asu*-ACR-16 (Fig. S4A) and is the only crystal structure of a protein homologous to *Asu*-ACR-16 co-crystalized with nicotine to date. The ligand-binding site for agonist is at the interface between the principal side and the complementary side in two adjacent subunits of nAChRs (Li et al., 2011; Rucktooa et al., 2012).

Nicotine adopts the same binding pose in all five ligand-binding sites in *Lst*-AChBP pentamer (Fig. 1A). The pyrrolidine ring of nicotine is oriented toward the basal side of the binding site on the principal subunit, whereas the pyridine ring faces the apical side on the complementary subunit. The protonated nitrogen (N2) in the pyrrolidine ring of nicotine is involved in cation-π interactions, mainly with W143 (on principal subunit) or maybe four aromatic

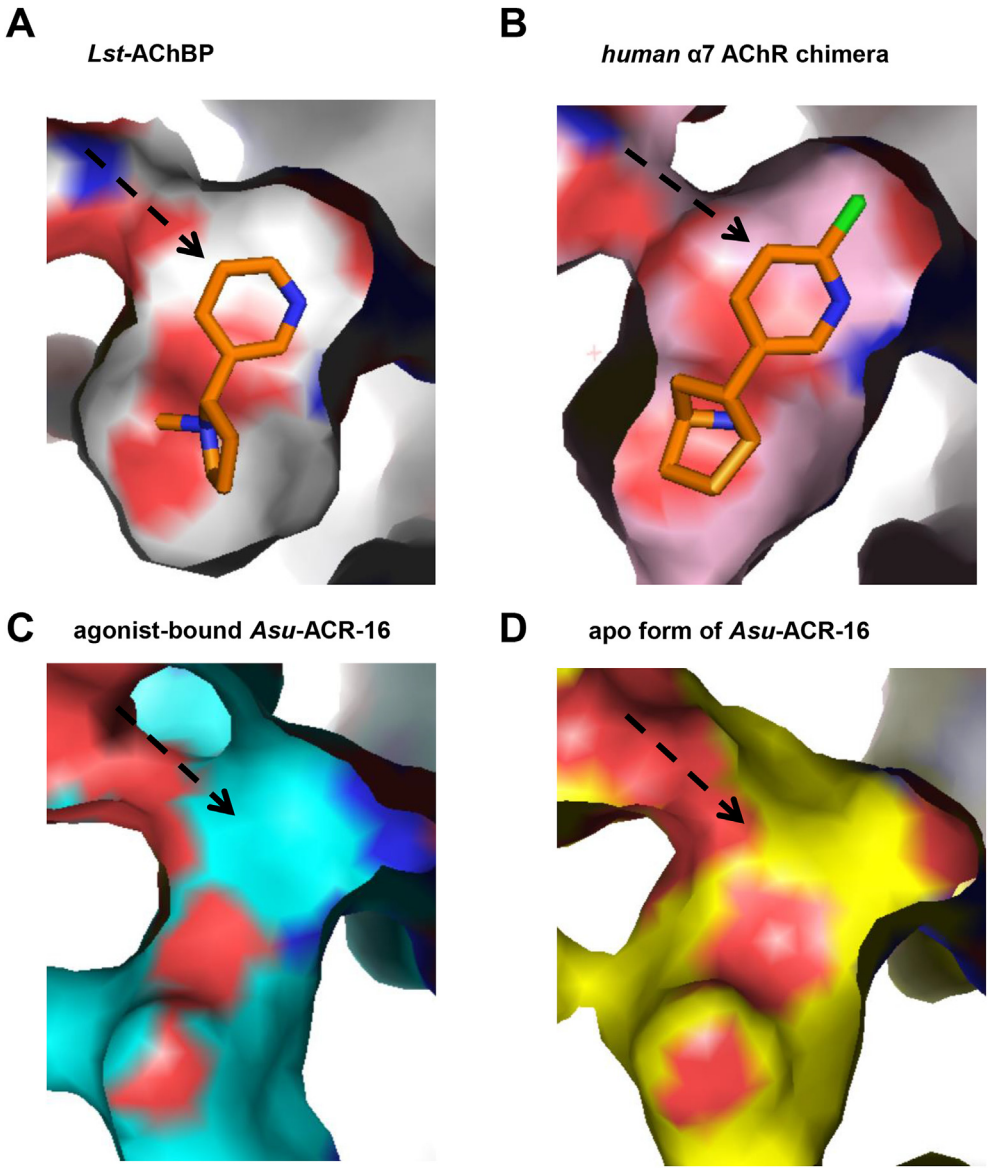

Fig. 2. Ligand-binding sites of *Asu*-ACR-16 and its homologous proteins.
(A) Surface representation in the open-up ligand-binding site of *Lst*-AChBP in complex with nicotine (PDB code: 1UW6). Oxygen-rich area (red), nitrogen-rich area (blue) and carbon-rich area (gray) are displayed. Empty space was observed around the 5-pyridine ring of nicotine, which suggests that the ligand-binding site is in favor of the linear functional group linking toward the 5-pyridine ring of nicotine. Little space is found around the pyrrolidine ring of nicotine.
(B) Surface representation in the open-up ligand-binding site of human α7 AChR chimera in complex with epibatidine (PDB code: 3SQ6), viewed by the same angle as (A). Oxygen-rich area (red), nitrogen-rich area (blue), carbon-rich area (pink) and chloride (green) are displayed. The azabicyclic ring N1 of epibatidine was superimposed with the pyrrolidine ring N2 of nicotine, while the pyridine ring N2 of epibatidine was superimposed with the pyridine ring N1 of nicotine.
(C) Surface representation in the open-up ligand-binding site of agonist-bound *Asu*-ACR-16 model, viewed by the same angle as (A). Oxygen-rich area (red), nitrogen-rich area (blue) and carbon-rich area (cyan) are displayed. Assuming the nicotine has the same binding pose as in (A) within the agonist-bound *Asu*-ACR-16, empty space around the 5-pyridine ring and pyrrolidine ring of nicotine, which allows nicotinic derivatives with modification in these positions fit into to the binding site. The black arrow indicates the likely orientation of the 5-pyridine ring moiety. (D) Surface representation in the open-up ligand-binding site of apo form *Asu*-ACR-16 model, viewed by the same angle as (A). Oxygen-rich area (red), nitrogen-rich area (blue) and carbon-rich area (yellow) are displayed. Assuming the nicotine has the same binding pose as in (A) within apo form *Asu*-ACR-16, there would be empty space around the 5-pyridine ring and pyrrolidine ring of nicotine, which would make the nicotinic derivatives with modification in these positions fit in the binding site. (For interpretation of the references to colour in this figure legend, the reader is referred to the web version of this article.)

residues in the binding site (principal subunit: Y89, Y185, Y192; complementary subunit: W53) (Fig. 1B). The N2 is also hydrogen-bonded to the hydroxyl moiety of Y89 and W143 carbonyl backbone. Hydrophobic interactions from disulfide-bonded C187 and C188 on loop C stabilize nicotine in the binding pocket. The pyridine ring nitrogen of nicotine (N1) is hydrogen-bonded to a water molecule, which is stabilized by the carbonyl backbone of L102 and M114 amide backbone of the complementary subunit (Fig. 1B) (Celie et al., 2004; Van Arnam and Dougherty, 2014).

Fig. 1C shows the ligand-binding site of the agonist-bound *Asu*-ACR-16 dimer viewed from the same angle as Fig. 1B. The residues involved in the binding site are highlighted in Fig. 1C and indicated in Fig. S4A by arrows. The interacting residues in the binding site of the agonist-bound *Asu*-ACR-16 model share similar orientations with those in the binding site of *Lst*-AChBP. The hydrophobic, hydrogen-bond and van der Waals contacts between nicotine and AChBP were therefore predicted in *Asu*-ACR-16. Y117, W173, Y214, Y221 from principal and W79 from complementary constitute the aromatic cage, in which W173 contributes most to the cation-π interaction with protonated tertiary amine or tetramethyl ammonium salt of nicotine or its derivatives. The hydroxyl moiety of Y117 and W173 carbonyl backbone are hydrogen-bonded to the protonated tertiary amine or ammonium of the ligand. The carbonyl backbone of N131 and I143 amide backbone from the complementary face have water-mediated hydrogen bond with the pyridine ring N1 of the ligand.

Structural superimposition of the binding-site residues among three different bound forms Asu-ACR-16 show details of conformational changes of residues when the agonist is in the binding pocket of the receptor. Of particular note is the inward movement of vicinal cysteines toward pyrrolidine N2 of nicotine. The antagonist-bound model has less steric hindrance in the open receptor binding site (Fig. 1D) (Huang et al., 2013).

The human α7 nAChR chimera (PDB code: 3SQ6) (Li et al., 2011) shows 62.98% sequence identity and 80.29% nucleotide sequence similarity with the extracellular domain of human α7 nAChR (UniProtKB accession number: P36544). The residues constituting the ligand-binding site are highly conserved between human α7 nAChR chimera and human α7 nAChR (Fig. S4B). The crystal structure of human α7 nAChR chimera co-crystalized with epibatidine could be used to study the binding site of agonist-bound human α7 nAChR. Comparison of the binding sites in *Lst*-AChBP (Fig. 2A), human α7 nAChR chimera (Fig. 2B), agonist-bound *Asu*-ACR-16 (Fig. 2C) and apo form of *Asu*-ACR-16 (Fig. 2D) reveals that the 5-substituted pyridine derivatives of nicotine would be favorable, with more space for the binding site of the ECD-*Asu*-ACR-16, but not for the human α7 nAChR. The black dotted arrows mark the likely orientation of the functional group on the 5-pyridine moiety of nicotine (Fig. 2C and D). Additionally, our docking results show that the 5-substituted pyridine ring approaches close to the disulfide bonds of *Asu*-ACR-16 and that the pyrrolidine ring is twisted downward in the binding site (Fig. S5).

3.2. Potency of nicotine derivatives

Initially we tested a range of nicotine analogues (compounds labelled 3–5 & 7–17 in Table 2, Fig. 3) as agonists to further characterize the pharmacological profile of *Asu*-ACR-16 receptors by measuring agonist EC_{50}, I_{max} and n_H values. *The* EC_{50} for (S)-nicotine was 6.21 ± 0.56 μM and the I_{max} was 82.39 ± 2.52%, $N = 5$ (Table 2). (S)-nicotine is a potent agonist of *Asu*-ACR-16, but can also activate mammalian nAChRs and as an anthelmintic would also cause effects in the host (Chavez-Noriega et al., 1997). As a low-molecular-weight and water soluble molecule, (S)-nicotine was selected as our initial lead for further optimization (Bleicher et al., 2003). Using (S)-nicotine as a pharmacophore and the predicted three-dimensional structures of the *Asu*-ACR-16 ligand-binding site, we studied structure-activity relationships by measuring the EC_{50}, I_{max} and n_H values of the nicotine derivatives (Fig. 4, S6 and Table 2) on the *Asu*-ACR-16 receptor. The agonist dose-response relationships for ACh and (S)-nicotine (Fig. 5A), pyridine substituted nicotine derivatives (Fig. 5B) and the pyrrolidine substituted nicotine derivatives (Fig. 5C) are shown. The pyridine N1 methylated substituent [(S)-1-methylnicotium], the 5'-carbonylated pyrrolidine substituent [(S)-cotinine], and the piperidine N2 methylated substituent [N-methyl anabasine] did not act as agonists.

3.3. (S)-enantiomers are more potent

We compared the pharmacological profiles of (S)-anabasine and its racemic mixture on *Asu*-ACR-16 (Fig. S7). The EC_{50} of (S)-anabasine was significantly lower than the EC_{50} of its racemic mixture ($P < 0.05$, $N = 5$). The I_{max} of (S)-anabasine was slightly higher than that of its racemic mixture ($P > 0.05$, $N = 5$). These results are consistent with other published results that illustrate the higher intrinsic activities of (S)-enantiomer nicotine alkaloids rather than their (R)-enantiomer (Cosford et al., 2000). Therefore, subsequent synthesis of compounds was directed towards preparation of (S)-enantiomers.

Table 2
Pharmacological profiles of ACh, nicotine and fifteen nicotine derivatives. Results (mean ± S.E.M.) were expressed as the EC_{50} (μM), Hill slope (n_H) and maximum response (I_{max}, %), number of repeats of each agonist experiment ($N_{agonist}$). One oocyte was used in each replicate of experiment.

No:	Compound name	EC_{50} (μM)	n_H	I_{max} (%)	$N_{agonist}$
1:	(S)-5-ethynyl-anabasine	0.14 ± 0.01	1.81 ± 0.24	79.33 ± 3.75	5
2:	(S)-5- bromoanabasine	0.32 ± 0.03	4.19 ± 1.58	80.69 ± 2.87	5
3:	(S)eSIB 1508Y	0.37 ± 0.10	0.94 ± 0.04	100.1 ± 4.36	5
4:	5-methylnicotine	0.99 ± 0.17	2.09 ± 0.14	76.05 ± 1.22	5
5:	(S)-anabasine	1.26 ± 0.19	2.26 ± 0.20	84.82 ± 4.20	5
6:	(S)-5-bromonicotine	2.04 ± 0.12	2.46 ± 0.21	69.66 ± 3.28	5
7:	6-methylnicotine	6.13 ± 0.53	3.25 ± 0.24	69.74 ± 1.56	5
8:	(S)-nicotine	6.21 ± 0.56	3.39 ± 0.36	82.39 ± 2.52	5
9:	ACh	6.36 ± 0.49	2.93 ± 0.13	97.42 ± 0.93	5
10:	(S)-1'- methylnicotinium	10.25 ± 0.62	3.52 ± 0.26	93.38 ± 5.25	5
11:	(S)-nicotine-5-carboxaldehyde	11.51 ± 0.63	8.61 ± 4.04	62.20 ± 6.80	5
12:	6-AN	12.18 ± 0.29	10.10 ± 0.15	6.29 ± 0.62	5
13:	homonicotine	16.62 ± 1.44	6.78 ± 2.50	22.01 ± 1.39	5
14:	nornicotine	25.73 ± 4.71	3.25 ± 0.49	62.64 ± 3.42	5
15:	N-methyl anabasine	<100			
16:	(S)-1- methylnicotinium	<100			
17:	(S)-cotinine	<100			

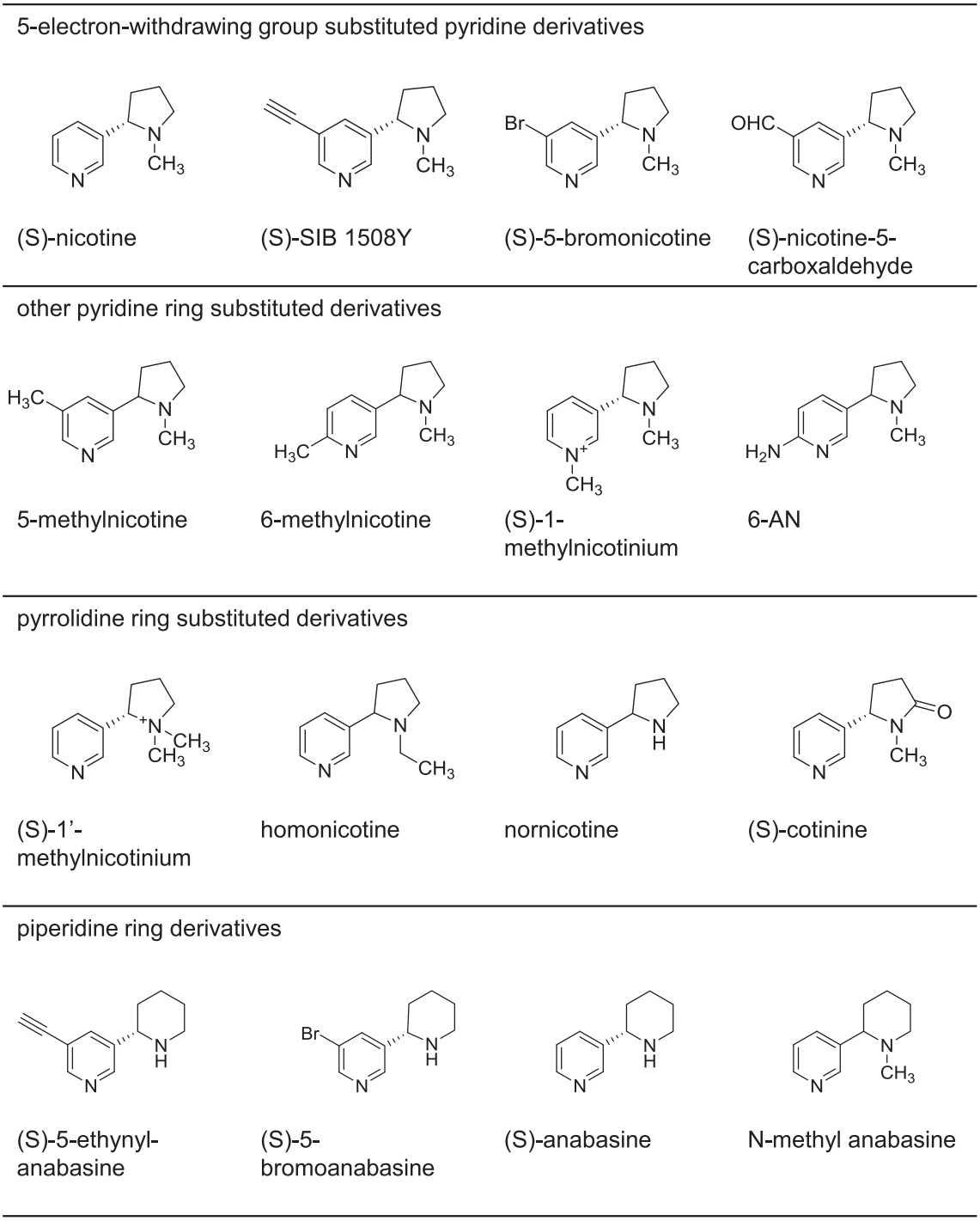

Fig. 3. Chemical structures of (S)-nicotine and fifteen derivatives studied. 5-substituted pyridine ring derivatives: (S)–SIB 1508Y, (S)-5-bromonicotine, (S)-nicotine-5-carboxaldehyde and 5-methylnicotine; other pyridine ring substituted derivatives: (S)-1-methylnicotinium, 6-methylnicotine and 5-(1-methyl-pyrrolidin-2-yl)-pyridin-2-ylamine (6-AN); pyrrolidine ring substituted derivatives: (S)-1'-methylnicotinium, homonicotine, nornicotine and (S)-cotinine; piperidine ring derivatives: (S)-5-ethynyl-anabasine, (S)-5-bromoanabasine, (S)-anabasine and N-methyl anabasine are shown.

3.4. (S) -5-ethynyl-anabasine, (S)-5-bromoanabasine and (S)-5-bromonicotine

Examination of the structures and EC_{50} potencies of (S)–SIB 1508Y and (S)-anabasine suggested that a novel compound, (S)-5-ethynyl-anabasine, would yield a more potent agonist. Consequently, it was synthesized, as described in the methods, along with (S)-5-bromonicotine and (S)-5-bromoanabsine that were produced during its synthesis. The three novel synthesized compounds were then tested on the *Asu*-ACR-16 receptor. The concentration response plots for these compounds revealed that two of the novel compounds, (S)-5-ethynyl-anabasine and (S)-5-bromoanabsine were the most potent agonists tested to date (Fig. 5C & Table 2).

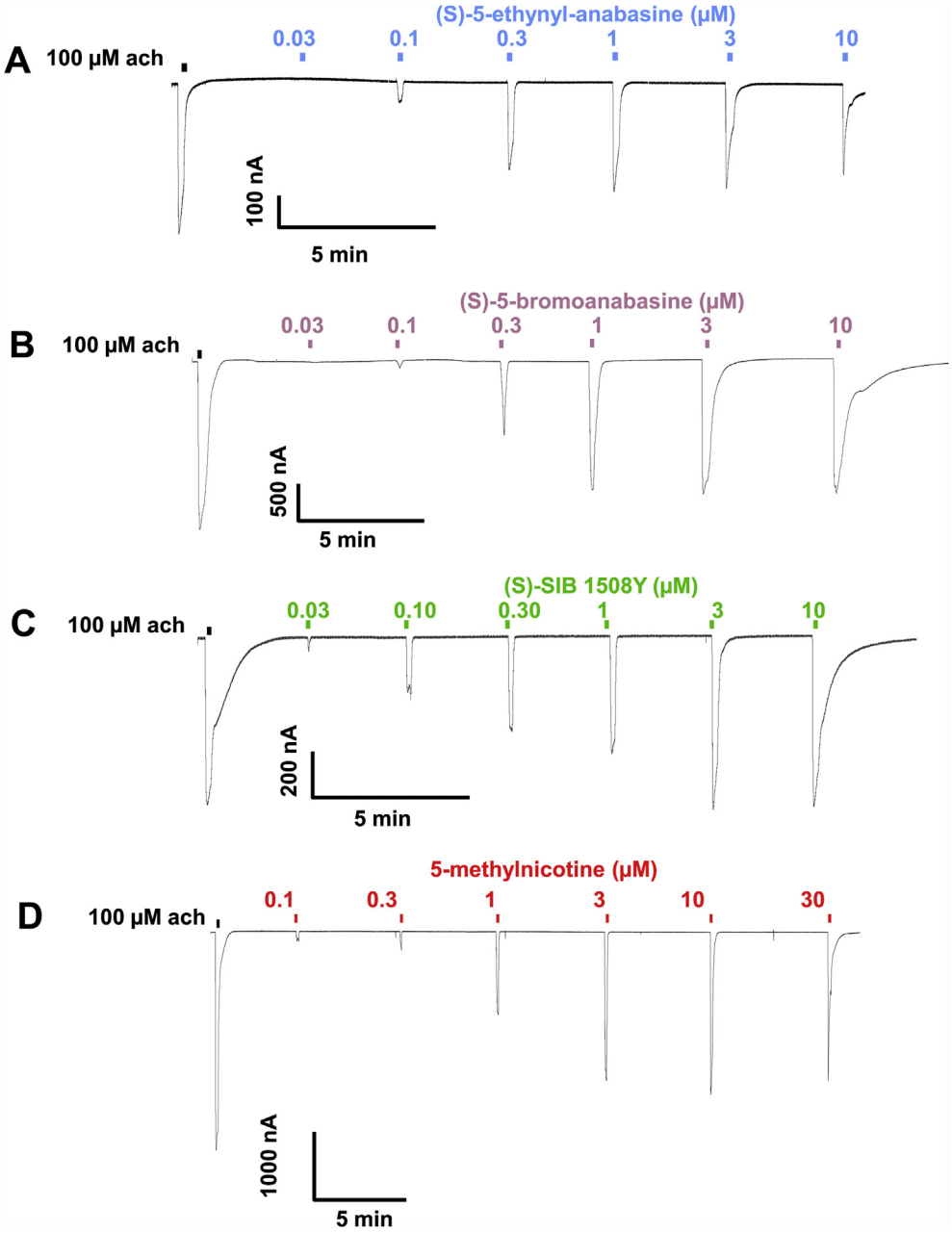

Fig. 4. Sample concentration-current recording traces for the most potent nicotine derivatives on the *Asu*-ACR-16 receptor. (S)-5-ethynyl-anabasine (A), (S)-5-bromoanabasine (B), (S)−SIB 1508Y (C), 5-methylnicotine (D) are depicted. For each nicotine derivative, 5 oocyte were tested as replicates. Resting membrane potential clamped at −60 mV. Downward responses to exposure of the agonists show opening of the ion-channel. Peak responses were recorded, normalized and fitted into the Hill equations.

3.5. Agonist rank order potency

Fig. 5 shows the dose-response plots for the most potent agonists. The rank order of potency the agonists based on the EC_{50} values, Table 2, was: (S)-5-ethynyl-anabasine > (S)-5-bromoanabasine ≈ (S)−SIB 1508Y > 5-methylnicotine ≈ (S)-anabasine > (S)-5-bromonicotine > 6-methylnicotine ≈ (S)-nicotine ≈ ACh > (S)-1'-methylnicotinium ≈ (S)-nicotine-5-carboxaldehyde ≈ 6-AN > homonicotine ≈ nornicotine. Two piperidine ring derivatives: (S)-5-bromoanabasine and (S)-anabasine, two 5-substituted pyridine derivatives: (S)−SIB 1508Y and 5-methylnicotine were more potent than ACh and (S)-nicotine ($P < 0.05$, $N = 5$). The EC_{50} of the novel lead compound, (S)-5-ethynyl-anabasine, is 44 times lower (more potent) than its initial pharmacophore, (S)-nicotine, and is the most potent agonist of *Asu*-ACR-16.

3.6. Correlation between affinity and potency among nicotine derivatives

The binding affinities of the selected nicotine derivatives were calculated for ligands docking into the agonist-binding site in the agonist-bound form, the apo (no ligand) form and the antagonist-bound form ECD-*Asu*-ACR-16 models. We examined the relationship between the binding affinities and the observed values of the expressed receptors for the EC_{50} (μM) of the nicotine derivatives. There was a positive correlation (+0.66) between the binding affinity and the EC_{50} of the apo form model ($P < 0.05$) (Fig. 6); the correlation with the agonist bound *Asu*-ACR-16 (0.36) and antagonist bound *Asu*-ACR-16 (0.46) were smaller and did not reach

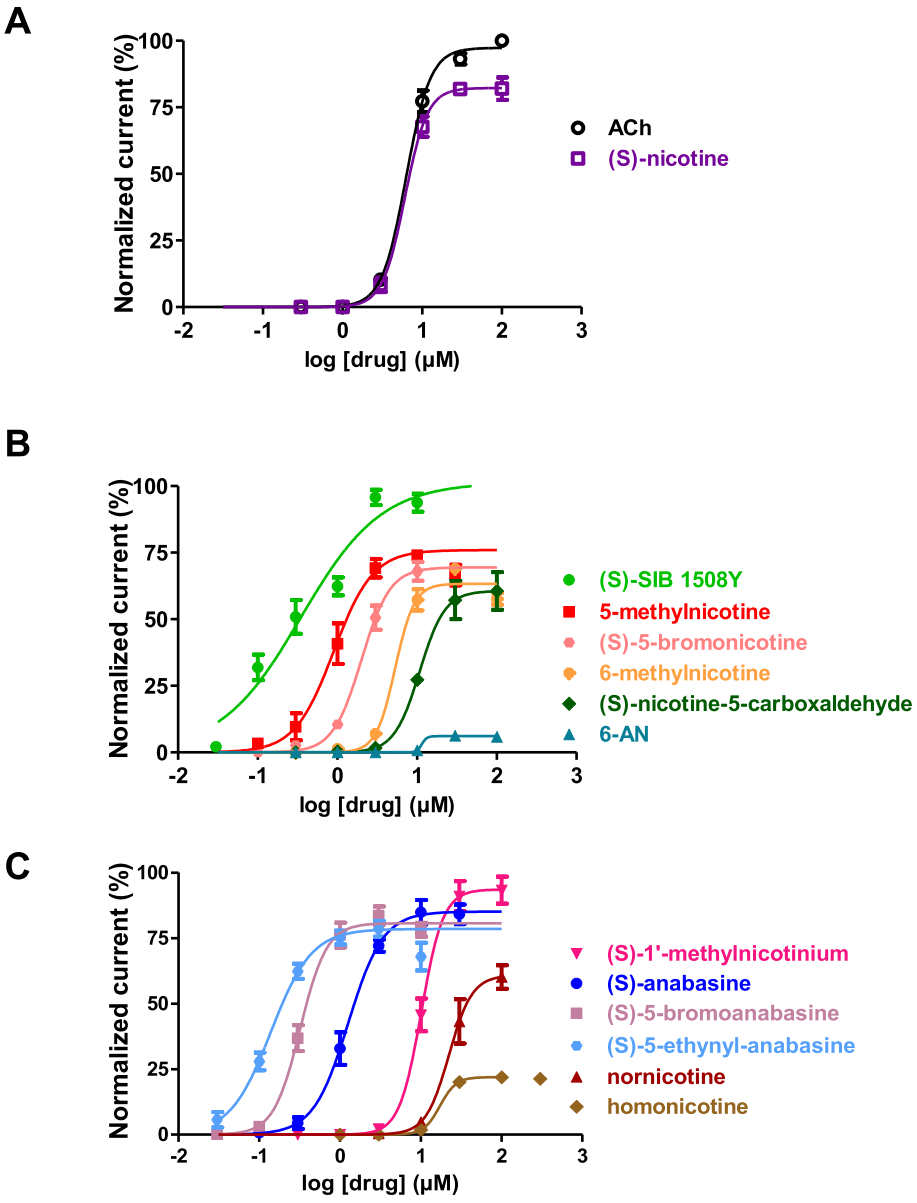

Fig. 5. Dose-response curves of nicotine derivatives for *Asu*-ACR-16. For experiment of each nicotine derivative, one oocyte was used as a group. Five replicates were performed for each group. Current responses are normalized to the first 100 μM control application (Methods).
(A) ACh and (S)-nicotine as two controls.
(B) Pyridine ring substituted derivatives. Responses of 30 μM 5-methylnicotine and 100 μM 6-methylnicotine are shown but were not included for fitting the Hill equation to estimate EC_{50}, n_H *and* I_{max} correspondingly due to their inhibitory effects at high concentrations.
(C) Pyrrolidine ring substituted derivatives. Response of 300 μM homonicotine is shown but was not included for fitting the Hill equation to estimate EC_{50}, n_H *and* I_{max} due to its inhibitory effect at high concentration.

statistical significance ($P > 0.05$). The highest correlation with the apo form suggests that this model is more likely to predict the potency of unknown agonists than the other models of the receptor.

4. Discussion

4.1. Structure-activity relationships of nicotine derivatives on Asu-ACR-16

4.1.1. Pyridine ring substituted derivatives

We studied the effects of functional groups added to the different positions of pyridine moiety of nicotine: the methyl group substituted at the 5- or 6- or N-pyridine moiety of nicotine, and an amino group substituted at the 6-pyridine moiety of nicotine. 5-Methylnicotine was the most potent agonist, while 6-methylnicotine was slightly less potent. 6-AN showed little agonist activity. The electron-donating group of the methyl or the amino at the 5- or 6-pyridine increased the electronegativity and alkalinity of the pyridine N1, and so stabilized the water-mediated hydrogen bond with the carbonyl backbone of N131 and I143 amide backbone from the complementary subunit of the receptor. The lone pair electrons on the pyridine N1 of (S)-1-methylnicotinium were replaced by the methyl group. As a result N1 cannot hydrogen-bond with the carbonyl backbone of N131 and I143 amide backbone from the receptor so that this reduces the intrinsic activity of N-pyridine substituted derivatives.

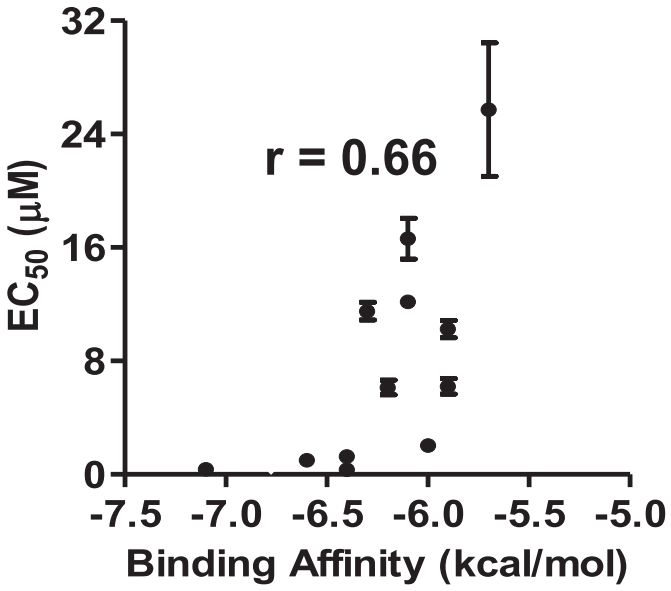

Fig. 6. Correlations between binding affinities (kcal/mol) of each derivative in the apo form *Asu*-ACR-16 and EC_{50} (μM) (A), binding affinities (kcal/mol) for the selected nicotine derivatives. The correlation coefficients (r) was used for evaluating the linear regression between affinities and pharmacological parameters ($r = 0.66$, $P < 0.05$).

4.1.2. 5-substituted pyridine derivatives

Given that the electron-donating groups at the 5-pyridine of nicotine were found to have the highest potency as agonists, the electron-withdrawing groups of acetylene, bromine or aldehyde derivatives at the 5-pyridine position of nicotine were selected for testing. (S)−SIB 1508 was the most potent agonist, while (S)-5-bromonicotine and (S)-nicotine-5-carboxaldehyde were less potent. The extra cavity within the binding site of *Asu*-ACR-16 agonist-bound and apo model could accommodate the linear acetylene substituent and globular bromine atom at the 5-pyridine ring of nicotine, allowing the ligands to extend into unoccupied space (Fig 2CD, top left quadrants of the binding pocket). The bent structure of aldehyde appears to be less favored in the binding pocket. Our docking studies show another possible reason for the 5-substituted pyridine derivatives to stabilize *Asu*-ACR-16. Fig. S5B&C show that the 5-substituted pyridine ring approaches towards the close-in conformation of the vicinal cysteines, which is a typical feature of the activated state of AChRs.

4.1.3. Pyrrolidine ring substituted derivatives

To study the effects of functional groups added to the different positions of pyrrolidine moiety of nicotine, a methyl or ethyl group was added at the N-pyrrolidine moiety of nicotine, and a ketone group was added at the 5'-pyrrolidine moiety of nicotine. The additional methyl group linked to the pyrrolidine N2 of (S)-1'-methylnicotinium produces a quaternary ammonium, which increases the cation-π interaction with the five aromatic residues from the ACR-16 receptor, but increases the steric hindrance around the pyrrolidine N2 making this compound stereochemically unfavorable. The increased steric hindrance due to the ethyl group at pyrrolidine N2 of homonicotine may be the reason for its reduced agonist potency. The secondary amine of nornicotine reduces the alkalinity and the probability of making a cation-π interaction with the receptor. The conjugative effect of the lone pair of electrons on the pyrrolidine N2 of (S)-cotinine to the π bond of carbonyl group, causes the pyrrolidine N2 to be hardly protonated, which significantly limits the cation-π interaction with the aromatic cage from the receptor and its action as an agonist.

4.1.4. Piperidine ring derivatives

The N-methyl pyrrolidine moiety was replaced by an N-methyl piperidine ring in nicotine structure to study the effect of increasing the membrane ring on the stimulatory activity of *Asu*-ACR-16. We found that N-methyl anabasine was inactive, but when the N-methyl group of the piperidine moiety was removed, the compound was a potent agonist. The piperidine ring of (S)-anabasine may have sterically and electrostatically stabilized the aromatic cage on the receptor better than the N-methylated pyrrolidine ring of nicotine. The novel lead compound, (S)-5-ethynyl-anabasine contains two moieties favorable to the *Asu*-ACR-16 ligand-binding site: an electron-withdrawing group at the 5-pyridine of nicotine moiety ((S)−SIB 1508Y) and; the piperidine moiety ((S)-anabasine). (S)-5-ethynyl-anabasine shows high potency (EC_{50} 0.14 ± 0.01 μM, $N = 5$) as an agonist.

4.2. Docking study as a probe for searching potent Asu-ACR-16 agonist

The potency (EC_{50}) of the selected nicotinic alkaloids was correlated more with the binding affinity in the apo model of *Asu*-ACR-16 than with the agonist- or antagonist-bound model of *Asu*-ACR-16. This appears to be due to the different conformation changes of vicinal cysteines or the opened-up orientation of W79 in the agonist-bound and antagonist-bound models of *Asu*-ACR-16, which reduces the cation-π interaction between W79 and nicotine N2 (Blum et al., 2010; Van Arnam and Dougherty, 2014). The statistical correlation between the predicted ligand binding affinities in the apo model of *Asu*-ACR-16 and their corresponding potencies (EC_{50}), suggests that the apo model would be more helpful when searching for potent agonists by docking.

5. Conclusion

We used structural models of the ECD-*Asu*-ACR-16 agonist-binding site and expressed receptor to study the structure-activity relationships of several nicotine alkaloids on *Asu*-ACR-16 receptor. We synthesized a novel compound, (S)-5-ethynyl-anabasine, which was 44 times more potent than (S)-nicotine as an *Asu*-ACR-16 agonist. Our structure-based drug discovery of ACR-16 agonists also suggests several other nicotine alkaloids as leads for further development.

Authorship contributions

Participated in research design: Zheng, Du, Robertson, VanVeller, and Martin.

Conducted experiments: Zheng, and Du.

Contributed new reagents or analytic tools: VanVeller, Yu, Martin, and Robertson.

Performed data analysis: Zheng, Chou and Du.

Wrote or contributed to the writing of the manuscript: Zheng, Du, Robertson, VanVeller, and Martin.

Statement of conflict of interest

The authors declare no competing interest in this work.

Acknowledgements

This research was supported by the Iowa State University startup to BV, NIH R21AI121831-01 to APR, NIH R01AI047194 to RJM.

Appendix A. Supplementary data

Supplementary data related to this article can be found at http://dx.doi.org/10.1016/j.ijpddr.2016.12.001.

References

Abongwa, M., Buxton, S.K., Courtot, E., Charvet, C.L., Neveu, C., McCoy, C.J., Verma, S., Robertson, A.P., Martin, R.J., 2016. Pharmacological profile of Asu-ACR-16, a new homomeric nAChR widely distributed in *Ascaris* tissues. Br. J. Pharmacol. 173, 2463–2477.

Arias, H.R., 2000. Localization of agonist and competitive antagonist binding sites on nicotinic acetylcholine receptors. Neurochem. Int. 36, 595–645.

Beng, T.K., Gawley, R.E., 2011. Application of catalytic dynamic resolution of N-Boc-2-lithiopiperidine to the asymmetric synthesis of 2-aryl and 2-vinyl piperidines. Org. Lett. 13, 394–397.

Bleicher, K.H., Bohm, H.-J., Muller, K., Alanine, A.I., 2003. Hit and lead generation: beyond high-throughput screening. Nat. Rev. Drug Discov. 2, 369–378.

Blum, A.P., Lester, H.A., Dougherty, D.A., 2010. Nicotinic pharmacophore: the pyridine N of nicotine and carbonyl of acetylcholine hydrogen bond across a subunit interface to a backbone NH. Proc. Natl. Acad. Sci. U. S. A. 107, 13206–13211.

Celie, P.H., van Rossum-Fikkert, S.E., van Dijk, W.J., Brejc, K., Smit, A.B., Sixma, T.K., 2004. Nicotine and carbamylcholine binding to nicotinic acetylcholine receptors as studied in AChBP crystal structures. Neuron 41, 907–914.

Chavez-Noriega, L.E., Crona, J.H., Washburn, M.S., Urrutia, A., Elliott, K.J., Johnson, E.C., 1997. Pharmacological characterization of recombinant human neuronal nicotinic acetylcholine receptors h alpha 2 beta 2, h alpha 2 beta 4, h alpha 3 beta 2, h alpha 3 beta 4, h alpha 4 beta 2, h alpha 4 beta 4 and h alpha 7 expressed in Xenopus oocytes. J. Pharmacol. Exp. Ther. 280, 346–356.

Cosford, N.D.P., Bleicher, L., Vernier, J.-M., Chavez-Noriega, L., Rao, T.S., Siegel, R.S., Suto, C., Washburn, M., Lloyd, G.K., McDonald, I.A., 2000. Recombinant human receptors and functional assays in the discovery of altinicline (SIB-1508Y), a novel acetylcholine-gated ion channel (nAChR) agonist. Pharm. Acta Helvetiae 74, 125–130.

de Silva, N.R., Brooker, S., Hotez, P.J., Montresor, A., Engels, D., Savioli, L., 2003. Soil-transmitted helminth infections: updating the global picture. Trends Parasitol. 19, 547–551.

Dougherty, D.A., 2013. The cation-pi interaction. Accounts Chem. Res. 46, 885–893.

Garcia, C.M., Sprenger, L.K., Ortiz, E.B., Molento, M.B., 2016. First report of multiple anthelmintic resistance in nematodes of sheep in Colombia. An. Acad. Bras. Ciencias 88, 397–402.

Holden-Dye, L., Joyner, M., O'Connor, V., Walker, R.J., 2013. Nicotinic acetylcholine receptors: a comparison of the nAChRs of Caenorhabditis elegans and parasitic nematodes. Parasitol. Int. 62, 606–615.

Huang, S., Li, S.-X., Bren, N., Cheng, K., Gomoto, R., Chen, L., Sine, S.M., 2013. Complex between α-bungarotoxin and an α7 nicotinic receptor ligand-binding domain chimaera. Biochem. J. 454, 303–310.

Li, S.-X., Huang, S., Bren, N., Noridomi, K., Dellisanti, C.D., Sine, S.M., Chen, L., 2011. Ligand-binding domain of an [alpha]7-nicotinic receptor chimera and its complex with agonist. Nat. Neurosci. 14, 1253–1259.

Liskey, C.W., Liao, X., Hartwig, J.F., 2010. Cyanation of arenes via iridium-catalyzed borylation. J. Am. Chem. Soc. 132, 11389–11391.

Mongan, N.P., Jones, A.K., Smith, G.R., Sansom, M.S., Sattelle, D.B., 2002. Novel alpha7-like nicotinic acetylcholine receptor subunits in the nematode Caenorhabditis elegans. Protein science. a Publ. Protein Soc. 11, 1162–1171.

Proskocil, B.J., Sekhon, H.S., Jia, Y., Savchenko, V., Blakely, R.D., Lindstrom, J., Spindel, E.R., 2004. Acetylcholine is an autocrine or paracrine hormone synthesized and secreted by airway bronchial epithelial cells. Endocrinology 145, 2498–2506.

Rucktooa, P., Haseler, C.A., van Elk, R., Smit, A.B., Gallagher, T., Sixma, T.K., 2012. Structural characterization of binding mode of smoking cessation drugs to nicotinic acetylcholine receptors through study of ligand complexes with acetylcholine-binding protein. J. Biol. Chem. 287, 23283–23293.

Rucktooa, P., Smit, A.B., Sixma, T.K., 2009. Insight in nAChR subtype selectivity from AChBP crystal structures. Biochem. Pharmacol. 78, 777–787.

Sixma, T.K., Smit, A.B., 2003. Acetylcholine binding protein (AChBP): a secreted glial protein that provides a high-resolution model for the extracellular domain of pentameric ligand-gated ion channels. Annu. Rev. biophysics Biomol. Struct. 32, 311–334.

Taly, A., Corringer, P.-J., Guedin, D., Lestage, P., Changeux, J.-P., 2009. Nicotinic receptors: allosteric transitions and therapeutic targets in the nervous system. Nat. Rev. Drug Discov. 8, 733–750.

Taylor, H.L., Spagnoli, S.T., Calcutt, M.J., Kim, D.Y., 2016. Aberrant Ascaris suum nematode infection in cattle, Missouri. USA. Emerg. Infect. Dis. 22, 339–340.

Trott, O., Olson, A.J., 2010. AutoDock Vina: improving the speed and accuracy of docking with a new scoring function, efficient optimization, and multithreading. J. Comput. Chem. 31, 455–461.

Van Arnam, E.B., Dougherty, D.A., 2014. Functional probes of drug-receptor interactions implicated by structural studies: cys-loop receptors provide a fertile testing ground. J. Med. Chem. 57, 6289–6300.

Wang, J., Czech, B., Crunk, A., Wallace, A., Mitreva, M., Hannon, G.J., Davis, R.E., 2011. Deep small RNA sequencing from the nematode Ascaris reveals conservation, functional diversification, and novel developmental profiles. Genome Res. 21, 1462–1477.

Zheng, F., Robertson, A.P., Abongwa, M., Yu, E.W., Martin, R.J., 2016. The Ascaris suum nicotinic receptor, ACR-16, as a drug target: four novel negative allosteric modulators from virtual screening. International Journal for Parasitology: Drugs Drug Resist. 6, 60–73.